Flame control by low-temperature hydrogen injection in a trapped vortex combustor

De Lauso, Vittorio; Mazzei, Lorenzo; Langella, Ivan

DOI
10.1016/j.proci.2025.105865

Publication date
2025

Document Version
Final published version

Published in
Proceedings of the Combustion Institute

Proceedings of the Combustion Institute 41 (2025) 105865

Contents lists available at ScienceDirect

Proceedings of the Combustion Institute

journal homepage: www.elsevier.com/locate/proci

Flame control by low-temperature hydrogen injection in a trapped vortex combustor

Vittorio De Lauso [a,*], Lorenzo Mazzei [b], Ivan Langella [a]

[a] Faculty of Aerospace Engineering, TU Delft, Kluyverweg 1, Delft, 2629 HS, The Netherlands
[b] Ergon Research s.r.l., via Campani 50, Florence, 50127, Italy

ARTICLE INFO

Keywords:
Low-temperature hydrogen combustion
Trapped vortex combustor

ABSTRACT

The transition to hydrogen as a primary fuel in aviation requires innovative strategies to mitigate challenges associated with flashback in combustion systems. Due to its low volumetric energy density, hydrogen is preferably stored at cryogenic temperatures ($T \leq 100$ K). Since stoichiometric hydrogen/air laminar premixed flames have been observed to sustain combustion even at temperatures as low as 100 K, low-temperature injection can be used as a strategy to control flashback and stabilize the flame. This study investigates the performance of low-temperature rich premixed hydrogen/air combustion within a model Rich-Quench-Lean (RQL) combustor configuration equipped with a Trapped Vortex Cavity (TVC). Large Eddy Simulations (LES) with Eulerian Stochastic Field (ESF) approach are conducted for this purpose. The LES are first validated against a recent experimental campaign involving high-speed chemiluminescence diagnostics. Subsequently, parametric studies explore the operating limits and flashback resistance of rich hydrogen flames under varying low-temperature conditions. Results indicate a strong sensitivity of the flame position within the TVC to the injection temperature. The strong reduction in laminar flame speed observed in experiments, however, is counteracted by the increase in turbulent/laminar flame speed ratio, adding to the complexity of the problem. Insights on how to control the flame dynamics in the cavity are provided within this study with the purpose of optimizing RQL-TVC designs for robust, low-emission, and flashback-resistant operation in hydrogen-based propulsion systems.

1. Introduction

The aviation sector is transitioning toward sustainable propulsion technologies, with hydrogen emerging as a promising fuel due to its high specific energy and zero-carbon emissions. Among advanced combustion concepts, Trapped Vortex Combustors (TVCs) have gained attention for their ability to enhance flame anchoring, reduce pressure losses, and improve overall efficiency. For a review on the different generations of TVC through experimental and numerical evaluations, the reader is referred to [1]. Unlike swirl-stabilized combustors, which can suffer from stability issues due to the significantly different thermophysical properties of hydrogen as compared to hydrocarbon fuels [2], TVCs provide robust flame-holding capabilities, making them an attractive option for aero-engine applications [3].

A critical challenge in TVCs is the high thermal load imposed on combustor walls, which is further exacerbated by the higher adiabatic flame temperature of hydrogen. This not only intensifies wall heating but also promotes NOx formation, particularly through the thermal NOx (Zeldovich) mechanism. Given the stringent emission regulations in aviation, mitigating NOx production in hydrogen-fueled gas turbines remains a key research priority. Until now only blended hydrocarbon-hydrogen-fueled TVC have been developed, mainly in lean-premixed configurations [4]. One promising strategy to balance performance and emissions is the Rich-Quench-Lean (RQL) TVC configuration, which has been extensively investigated for hydrocarbon fuels [5].

Computational fluid dynamics (CFD) has become in recent years increasingly popular as opposed to expensive experiments to aid the design of innovative configurations. In particular, large eddy simulations (LES) provide a high-fidelity approach for modeling turbulent reacting flows, where rate-controlling processes such as molecular transport and chemical reactions occur at the smallest, unresolved scales. Several models have been proposed to capture the interaction between turbulent wrinkling and combustion at the unresolved scales, and a review can be found in [6]. Moreover, for hydrogen combustion modeling, additional challenges arise due to hydrogen's high diffusivity, low molecular weight, and strong preferential diffusion effects, which can significantly impact the turbulence-chemistry interactions (TCIs).

* Corresponding author.
E-mail address: v.delauso@tudelft.nl (V. De Lauso).

https://doi.org/10.1016/j.proci.2025.105865
Received 1 May 2025; Accepted 5 September 2025
Available online 10 October 2025

Capturing these effects accurately requires appropriate combustion models, particularly at cryogenic temperatures. Yang et al. [7] showed that the large expansion ratios at cryogenic conditions, combined with pressure wave interactions in a closed channel, enhance flame surface wrinkling via Darrieus–Landau (DL) and Rayleigh–Taylor (RT) instabilities, drastically accelerating the burning rate. Chen et al. [8] confirmed the presence of strong DL instabilities under such conditions and found that the increase in flame surface area is primarily driven by large-scale flame structures, which in turn raises the turbulent-to-laminar flame speed ratio relative to ambient-temperature flames. In the present work both a transported filtered density function (FDF) approach [9] with an Eulerian stochastic fields (ESF) closure, and the artificially thickened flame (ATF) model [10] approach are first used to investigate the influence of sub-grid scale (SGS) fluctuations on filtered reaction rates in a TVC configuration where experimental data is available for validation. In particular, the ESF approach is further used to investigate uncommon operative points where experimental data is not available and both premixed and diffusion flame modes are observed. In fact, the ESF approach enables a direct representation of the chemical source term in the filtered governing equations without depending on a specific regime (premixed) assumption [11].

The objective of this study is to characterize the stability of a rich premixed hydrogen flame at cryogenic temperatures within a TVC cavity, laying the groundwork for the development of a low-emission, high-efficiency hydrogen-fueled RQL-TVC. In particular, this study focuses on the rich flame within the cavity, where fuel-rich conditions could potentially suppress NOx formation while maintaining stable combustion. As this configuration allows for independent control of the cavity and main flow [1], the rich part of the RQL can be studied in isolation. More specifically, this study considers combustion at cryogenic temperatures (≈ 150 K), a regime that has been demonstrated to sustain hydrogen flames in both experimental [12] and numerical [8] investigations.

The paper is organized as follows: Section 2 outlines the governing equations, Section 3 details the considered geometry, numerical setup, and the development of the simulation matrix design. The findings are then presented in Section 4, followed by conclusions in Section 5.

2. Modeling

2.1. Governing equations

The Favre-filtered, density varying Navier–Stokes equations for multi-component reacting flows for mass and momentum conservation are:

$$\frac{\partial \overline{\rho}}{\partial t} + \frac{\partial \overline{\rho}\widetilde{u_i}}{\partial x_i} = 0 \tag{1}$$

$$\frac{\partial \overline{\rho}\widetilde{u_i}}{\partial t} + \frac{\partial \overline{\rho}\widetilde{u_i}\widetilde{u_j}}{\partial x_i} = -\frac{\partial \widetilde{p}}{\partial x_i} + \frac{\partial}{\partial x_i}\left(\mu \frac{\partial \widetilde{u_i}}{\partial x_i}\right) + \frac{\partial \tau_{sgs,ij}}{\partial x_i} \tag{2}$$

with $\widetilde{u_i}$ being the ith component of the filtered velocity and $\overline{\rho}$, μ and $\widetilde{p}$ the filtered mixture density, dynamic viscosity and pressure respectively. The Boussinesq hypothesis for the unresolved Reynolds stresses yields:

$$\tau_{sgs,ij} = -2\mu_{sgs}\left(\widetilde{S_{ij}} - \frac{1}{3}\delta_{ij}\widetilde{S_{kk}}\right)$$

with $\widetilde{S_{ij}}$ being the filtered rate-of-strain tensor, δ_{ij} the Kronecker delta and μ_{sgs} the eddy viscosity.

The Wall-Adapting Local Eddy-viscosity (WALE) model was applied in this work to close the sub-grid stresses as:

$$\mu_{sgs} = \overline{\rho}\left(C_w \Delta\right)^2 \frac{(s^d_{ij}s^d_{ij})^{2/3}}{(S_{ij}S_{ij})^{5/2} + (s^d_{ij}s^d_{ij})^{5/4}}$$

Table 1
DTFM flame parameter alterations.

	Unaltered flame	Thickened flame
Diffusivity	D_k	$E \cdot F \cdot D_k$
Flame Speed	s_L	$E \cdot s_L$
Flame Thickness	δ_L	$F \cdot \delta_L$

For a detailed explanation of the model coefficients, the reader is referred to the paper of Nicoud and Ducros [13].

The generic equation for the species mass fraction Y_k reads:

$$\frac{\partial \overline{\rho}\widetilde{Y_k}}{\partial t} + \frac{\partial \overline{\rho}\widetilde{u_i}\widetilde{Y_k}}{\partial x_i} = \frac{\partial}{\partial x_i}\left(\left(\overline{\rho}D_k + \frac{\mu_{sgs}}{Sc_t}\right)\frac{\partial \widetilde{Y_k}}{\partial x_i}\right) + \widetilde{\dot{\omega}_k} \tag{3}$$

where D_k is the diffusivity of species k, $Sc_t = 0.7$ is the subgrid Schmidt number and $\widetilde{\dot{\omega}_k}$ is the filtered reaction rate of species k. An equation for the specific sensible enthalpy $\widetilde{h_s}$ is also solved, which reads:

$$\frac{\partial \overline{\rho}\widetilde{h_s}}{\partial t} + \frac{\partial \overline{\rho}\widetilde{u_i}\widetilde{h_s}}{\partial x_i} = \frac{\partial \widetilde{p}}{\partial t} + \widetilde{u_i}\frac{\partial \widetilde{p}}{\partial x_i} + \widetilde{\dot{\omega}_T} + \frac{\partial}{\partial x_i}\left(\left(\lambda + \frac{\mu_{sgs}c_{p,mix}}{Pr_t}\right)\frac{\partial \widetilde{T}}{\partial x_i}\right) - \frac{\partial}{\partial x_i}\left(\overline{\rho}\sum_{k=1}^{N_{sp}} V_{k,i}\widetilde{Y_k}\widetilde{h_{s,k}}\right) \tag{4}$$

with N_{sp} being the number of species, $Pr_t = 0.7$ the subgrid Prandtl number, $\widetilde{\dot{\omega}_T}$ the heat release rate and $\widetilde{h_{s,k}}$ the sensible enthalpy of species k. Mixture thermal conductivity λ and dynamic viscosity μ are computed using Sutherland transport law [14], while the mixture specific heat at constant pressure, $c_{p,mix}$, is computed from JANAF polynomials. The species diffusion coefficient D_k and the diffusion velocity $V_{k,i}$ are obtained assuming constant Lewis number and Fick's law, respectively. A table of the Lewis numbers employed in this work is provided in the supplementary material. Mass conservation, which is no longer strictly valid due to the presence of non-unity Lewis numbers, is enforced by adjusting the N_2 mass fraction. While this approach is not ideal for accurate NO prediction, it is justified here because NO transport is not explicitly modeled; instead, NO formation is estimated based on flame surface calculations and 1D flame values. Finally, ideal gas law is implemented to relate the density-varying mixture to temperature, pressure and composition.

2.2. Combustion models

A closure model is needed for the filtered source terms in the species and energy equations. In this work a dynamic thickened flame model (DTFM), for which the details of the implementation follow the work of Legier et al. [10], and a transported Filtered Density Function (t-FDF) with Eulerian stochastic fields (ESF) have been employed. The former model is based on dynamically altering the nature of the flame front through an efficiency factor E and a local thickening factor F, allowing the flame front to be fully resolved by preserving the flame speed. In order to achieve this, diffusivity of species, laminar flame speed and flame thickness are modified as indicated in Table 1. This way the reaction rates can be modeled using the Arrhenius form, as for a direct numerical simulation. Further modeling details are omitted for brevity and can be found in [10].

The ESF approach describes the stochastic evolution of species and enthalpy by a composition FDF, which is a convoluted (using the LES filter kernel) PDF of said fields. The fine-grained composition PDF $P_{sgs}(\psi) = \Pi_{\alpha=1}^{n}\delta(\psi_a - \phi_a)$, with $\alpha = 1, \ldots, n$ scalar quantities represented

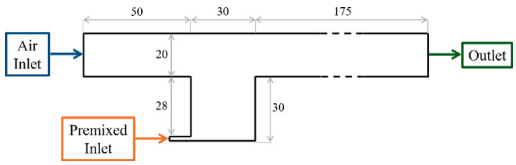

Fig. 1. Section of the test rig employed in the experiments found in [4]. Dimensions are given in mm. The out-of-the-plane width is 50 mm.

by ϕ_α, represents the probability of $\phi = \psi$. The FDF, or filtered PDF, $\widetilde{P}_{sgs}$, follows the transport equation:

$$\frac{\partial \overline{\rho}\widetilde{P}_{sgs}}{\partial t} + \frac{\partial \overline{\rho}\widetilde{u}_j \widetilde{P}_{sgs}}{\partial x_j} + \sum_{\alpha=1}^{n} \frac{\partial}{\partial \psi_\alpha}\left(\overline{\rho}\dot{\omega}_\alpha \widetilde{P}_{sgs}\right) = \frac{\partial}{\partial x_j}\left[\overline{\rho}\left(D_\alpha + D_t\right)\frac{\partial \widetilde{P}_{sgs}}{\partial x_j}\right] - \sum_{\alpha=1}^{n}\sum_{\beta=1}^{n} \frac{\partial^2}{\partial \psi_\alpha \psi_\beta}\left(\overline{\rho}\frac{\widetilde{\nu}}{Sc}\widetilde{\frac{\partial \phi_\alpha}{\partial x_i}\frac{\partial \phi_\beta}{\partial x_i}}|_{\phi=\psi}\widetilde{P}_{sgs}\right) \quad (5)$$

From left to right, terms in the above equation signify temporal evolution, convective transport, chemical source term, diffusion term (with both laminar D_α and turbulent D_t contributions of diffusivities). The last term corresponds to the molecular (micro-) mixing, which can be modeled using the interaction by exchange with the mean (IEM) approach, also known as linear mean square estimate (LMSE) [15].

In the ESF method, the FDF is decomposed into N_s stochastic fields, with ζ_α^n being the nth realization of the scalar ϕ_α. In particular, following the method proposed by Valiño et al. [16]:

$$d\overline{\rho}\zeta_\alpha^n + \frac{\partial \overline{\rho}\widetilde{u}_i \zeta_\alpha^n}{\partial x_j}dt - \frac{\partial}{\partial x_j}\left[\left(D_\alpha + D_t\right)\frac{\partial \zeta_\alpha^n}{\partial x_j}\right]dt = \overline{\rho}\sqrt{\frac{2\mu_{sgs}}{\overline{\rho}Sc_{sgs}}}\frac{\partial \zeta_\alpha^n}{\partial x_j}dW_j^n - \frac{\overline{\rho}}{2\tau_{sgs}}(\zeta_\alpha^n - \widetilde{\phi_\alpha})dt - \overline{\rho}\dot{\omega}_\alpha^n dt \quad (6)$$

It is necessary to point out that the solution of each stochastic field is not a physical realization of the real field, but rather an equivalent stochastic system to Eq. (5). The filtered value of the scalar can then be retrieved as the mean of its stochastic fields: $\widetilde{\phi}_\alpha = \frac{1}{N}\sum_{n=1}^{N_s}\zeta_\alpha^n$. The source of stochasticity of the field can be found in the Wiener process dW_j^n, resulting from the Itô integration of the SPDE, hereby approximated by the time-step increment as:

$$dW_j^n = \gamma_j\sqrt{dt}$$

With $\gamma_j = \{-1, 1\}$ being a random dichotomic vector with zero mean.

3. Methodology

3.1. Simulation setup

The geometry of the combustor follows the atmospheric TVC test rig employed in the experimental campaign by Verma et al. [4], for which a section view is given in Fig. 1.

A premixed fuel–air mixture, defined by fuel H_2 content in volume $H_{2\%,vol}$, equivalence ratio ϕ_{rich}, thermal power P_{th} and temperature T_{cavity}, is introduced through a 2 mm slot at the base of the cavity with velocity V_{cavity}, while the main airflow, at 300 K and with speed V_{main}, is supplied to the primary duct, which has a height of 20 mm. Turbulent inflow conditions are generated using the method described in [17], which prescribes the spatial integral length scales, mean velocity, and Reynolds stress tensor field. These quantities are extracted from a previously conducted auxiliary simulation of a fully developed corresponding channel flow. The TVC cavity has a width of 50 mm, and the combustion products exit the combustor at atmospheric pressure after traveling 175 mm downstream of the cavity.

Table 2
Simulation cases with preliminary results from 1D freely propagating flames: s_L^0 symbolizes the unstretched laminar flame speed, δ_L^0 the flame thickness, τ_L^0 the flame timescale, T_{ad} the adiabatic flame temperature and σ defines the ratio between density of reactants and products.

Symbol (units)	V	S1	S2	S3
ϕ_{rich} (–)	1.5	5	5	3
$H_{2\%,vol}$ (–)	50	100	100	100
P_{th} (kW)	13	10	10	10
T_{cavity} (K)	300	300	150	150
V_{cavity} (m/s)	34.06	15.02	7.51	9.13
V_{main} (m/s)	10.00	9.14	6.46	8.95
s_L^0 (m/s)	0.216	1.328	0.368	0.942
δ_L^0 (mm)	0.79	0.60	0.62	0.31
τ_L^0 (ms)	3.65	0.45	1.68	0.33
T_{ad} (K)	1989	1406	1281	1648
σ (–)	6.85	4.36	7.95	9.91
Y_{NO} (–)	6.19e−5	2.70e−8	1.30e−8	1.41e−7

Four simulations have been performed: one validation case (V) for a hydrogen/methane blend for which experimental data is available, and 3 parametric studies (S1, S2, S3), outlined in Table 2. Simulation S1 determines a baseline operating condition for a 100% H_2 operation, S2 explores the effect of lowering the injection temperature and S3 explores the effect of lowering the equivalence ratio at a low injection temperature. To predict realizable low-temperature setpoints employed in S2 and S3, perfect adiabatic premixing of H_2 at 50 K with atmospheric air at 300 K is assumed, resulting in a mixture temperature of approximately 150 K for the equivalence ratios considered, namely ϕ_{rich} = 3 and 5.

The adoption of such highly rich equivalence ratios stems from the results reported in [5]. While the TVC ensures stable flameholding, it does so at the cost of a long residence time in the cavity, which can markedly enhance NO formation. In addition, the cavity inevitably entrains a fraction of the surrounding mainflow air, further contributing to the presence of air at elevated temperatures. To counteract these effects, the present study seeks to reduce cavity temperatures, which is pursued through the combined use of cryogenic hydrogen/air premixing and highly rich equivalence ratios.

To reduce computational cost the reduced mechanisms DRM19 [18] (19 (+N2) species, 84 reactions) and the mechanism by Konnov [19] (8 (+N2) species, 28 reactions) have been used to describe the chemistry respectively for the blended and only hydrogen cases. The choice of the Konnov mechanism is motivated by its previous use and validation in low-temperature combustion simulations [8]. Further comparisons with more recent laminar flame speed measurements are presented in the Supplementary Material, demonstrating the suitability of this chemical mechanism, together with its thermodynamic and transport property databases, for modeling low-temperature rich premixed hydrogen/air combustion.

3.2. Numerical solver

The Navier–Stokes equations are discretized using the finite volume approach. Two finite-volume solvers have been used: a commercial software, CONVERGECFD [20], and an open-source software, OpenFOAM [21], respectively for the cases with DTFM and ESF models. Note that the first is only used for comparative purposes, given the limited amount of experimental data. In both cases the time derivatives are discretized using a first order implicit scheme. Gradients are discretized with a second order scheme, with a total variation diminishing limited linear scheme for the convective terms in order to avoid numerical instabilities in the region of strong gradients across the flame.

Given that hexahedral meshes have been used, Laplacian and surface normal gradient discretizations follow a second-order accurate orthogonal scheme. While for the first software, an adaptive mesh refinement (AMR) strategy has been employed, for the second software

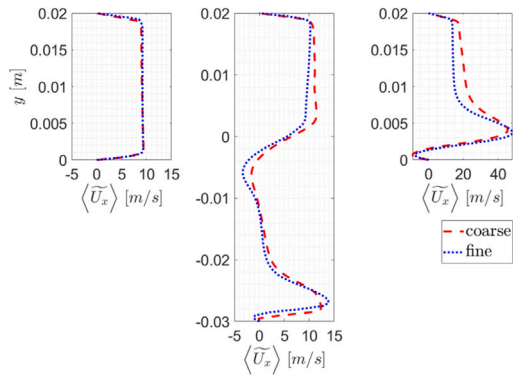

Fig. 2. Profiles of time averaged, LOS averaged axial velocity at different axial locations: before the cavity — $x = -15$ mm (left), within the cavity — $x = 15$ mm (center) and after the cavity — $x = 45$ mm (right).

two meshes have been employed to conduct a mesh refinement study: a coarse mesh with 0.25 million elements, with the typical cell length $\Delta \approx 0.5$ mm and a fine mesh with 2.25 million elements, with typical cell length $\Delta \approx 0.15$ mm in the cavity, ensuring a wall normal coordinate of $y^+ \approx 1$ and at least two cells within the laminar flame thickness for the most demanding case. Both meshes were observed to satisfy Pope's criterion for 80% turbulent kinetic energy. The following observations are based on case S1, displayed in Fig. 2, motivating the choice of the finer mesh; however, they apply to all simulations, with only the major trends reported here:

- The primary turbulent air inlet, modeled using the random spots method [17], exhibits negligible sensitivity to mesh refinement.
- At the cavity/main channel boundary, the intensity of the secondary vortex, with center located at a height of $y = -0.01$ m and identified through the time averaged, line of sight (LOS) averaged axial velocity $\langle \widetilde{U}_x \rangle$, increases with resolution, consequently influencing the interaction between the main flow and the secondary vortex, impacting the entrainment of air in the recirculating hot products.
- Similarly, the main vortex is affected by mesh resolution as the increased number of points inside the flame provides a more accurate representation of the rich premixed flame in the cavity.

Given that the coarser mesh proved unsatisfactory results in the validation process, underestimating the flame length relative to experimental results, the finer mesh was chosen for the simulations.

4. Results

4.1. Validation against experimental data

The ESF approach is first evaluated against experimental data [4]. To further assess the ability of the ESF model to predict the reacting physics in the cavity and thus reduce uncertainty, the results from the ESF approach are further compared to those obtained using the DTFM approach. Results from LES in terms of heat release rate (HRR) are compared to OH* measurements in Fig. 3. By examining the line-of-sight (LOS) integrated values of averaged HRR, the flame can be divided into three distinct regions, annotated in the left picture of Fig. 3:

1. A premixed flame front in the cavity
2. A premixed flame front in the main flow
3. A diffusion flame front in the cavity

The premixed flame front (1) presents limited to no wrinkling, and burns on the side of the injected jet. The second flame front (2) exhibits wrinkling as indicated by the more distributed region of HRR, which is attributed to vortex shedding from the shear layer between the trapped vortex and the main flow. According to the experiments reported in Fig. 3, this region presents increased flame reactivity, due to both wrinkling and air entrainment, and enhanced burning efficiency, as the flame burns at a lower equivalence ratio, closer to stoichiometry.

Regarding the last flame region (3), the ATF model is observed to better capture the spatial distribution of HRR as compared to the ESF model. Species analysis near the flame front reveals that this structure involves exclusively H_2 and air, forming a diffusion flame. The presence of H_2 in this region can be explained by two key factors: (i) Rich CH_4/H_2/air combustion produces H_2 as an intermediate species. This is supported by other experimental setpoints (not shown), where a methane-only case still exhibited a similar flame structure near the forebody; and (ii) high diffusivity of H_2, which causes it to migrate into this region.

Despite the ESF model with 4 fields does not fully capture the third flame region accurately, the transported FDF approach remains necessary due to its ability to account for flame regimes in the turbulence-chemistry interaction space that could suffer of modeling issues with the DTFM approach. Moreover, the focus of this analysis is placed on the rich premixed flame region, where the ESF model shows satisfactory results. For this reason, the ESF model is retained for the investigation presented in the next section.

4.2. Baseline design for H2-fueled RQL-TVC and effect of low temperature injection

When 100% of hydrogen is injected in the cavity, the reactive flow dynamics in the cavity changes significantly. This can be observed for the baseline case (case S1 of Table 2) in Fig. 4. In particular, due to its strong diffusivity, the excess hydrogen from the rich flame at the bottom of the cavity quickly migrates upstream towards the main air flow, creating a spurious, diffusion flame anchoring within the shear layer between cavity and airflow. Moreover, when the momentum flux ratio, defined as $J = (\rho_{\text{cavity}} U^2_{\text{cavity}})/(\rho_{\text{main}} U^2_{\text{main}})$, is kept to the value used for the validation case (case V of Table 2, $J = 10$), excessive oscillations in the region of the shear layer between cavity and main air flow are observed. This is due to the lower density of H_2 as compared to CH_4 and the higher equivalence ratio in case S1 as compared to case V, implying a significant reduction in the main flow velocity to achieve $J = 10$, resulting into a transition from a *deep* cavity to a *shallow* cavity behavior, according to the classification in [22]. For these reasons, the momentum flux in the baseline configuration (case S1) is changed from $J = 10$ to $J = 1$, which as shown in the figure is observed to be effective in stabilizing the vortex shedding dynamic in the shear layer between main flow and cavity. Note that, although undesired, the spurious diffusion flame is not the objective of the present work and is therefore not investigated further. The attachment points of rich premixed and diffusion flames are located on the cavity walls, which are assumed adiabatic for simplicity. To test the validity of this assumption, a sensitivity study on the cavity wall thermal boundary conditions was conducted. The results, reported in the Supplementary Material, show that flame-wall interaction effects become visible under non-adiabatic conditions. However, the core flame structure and the mean and standard deviations of velocity, pressure, and temperature in the rich premixed products remain largely unaffected, confirming that the assumption of adiabatic walls does not alter the main conclusions in the present study. The effect of low temperature injection in the cavity is instead studied next.

When the temperature of the H_2/air mixture at the inlet is reduced to 150 K (from case S1 to S2 of Table 2), a strong increase of flame wrinkling and heat release fluctuations are observed in the premixed flame (bottom of the cavity). This can be seen in Fig. 5, showing the HRR from the LES-ESF at different instants of time. This observation is

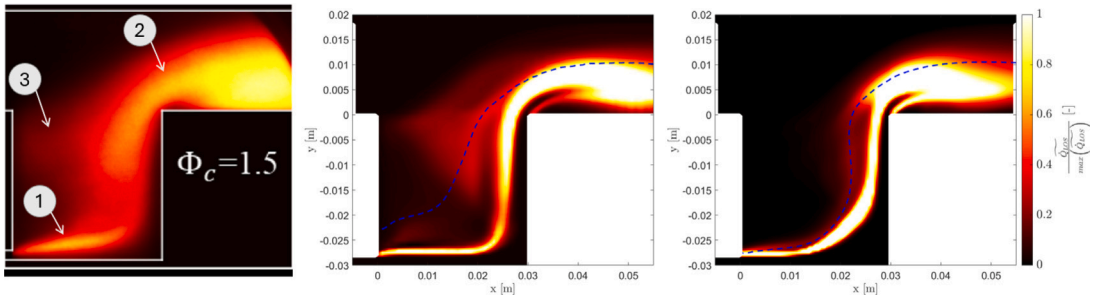

Fig. 3. Midplane contours of (left) experimental averaged OH* chemiluminescence [4], and normalized mean LOS HRR from LES employing (center) DTMF and (right) ESF approaches. The dashed line indicates the LOS averaged stoichiometric mixture level.

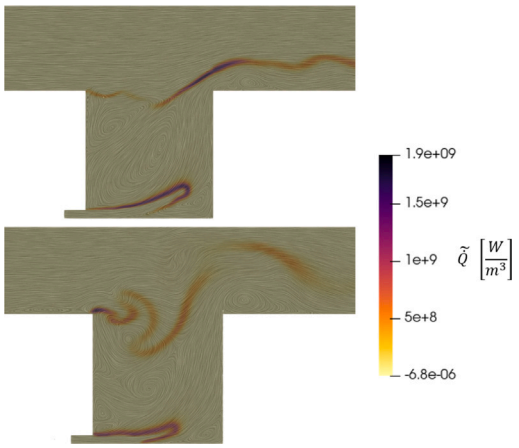

Fig. 4. Instantaneous Heat Release Rate contours on streamlines of velocity at a representative timestep. Top: J = 1. Bottom: J = 10.

consistent to those in [8], where the onset of flame instability was reported for low temperature injection. This large-scale wrinkling evolves following the steps shown in Fig. 5 in the following manner: at timestep t_0 (a), pockets of products from the recirculation region corrugate the flame front and penetrate into the reactants; (b) a bubble forms; and (c) the bubble detaches and the cycle restarts. This dynamics is associated to relatively large fluctuations of heat release and temperature (to be discussed later), and among the reactive cases it is only observed for case S2. Moreover, an additional non reactive simulation corresponding to the setpoint of S2 (not shown) was observed not to lead to any instability in the cavity, implying that the increased density of the colder reactants in case S2 as compared to S1 cannot explain alone the dynamics observed in Fig. 5. On the contrary, the increased density ratio σ, defined as $\sigma = \rho_{\text{reactants}}/\rho_{\text{products}}$, between reactants and products in the cavity, is observed to drive the wrinkling and unsteady dynamics observed for case S2. This in turn is associated with two mechanism for instability. The first is associated to the baroclinic vorticity. Vorticity is generated as the cold, denser reactant flow is injected alongside the hot, less dense products recirculating within the cavity. The density gradient in such a case is parallel to the cavity height. The pressure field, on the other hand, shows a gradient of pressure parallel to the cavity length, due to the impingement of the injected flow on the aft-body. The baroclinic vorticity production can be expressed as:

$$\frac{1}{\rho^2}\vec{\nabla}\rho \times \vec{\nabla}p \tag{7}$$

Gradients of density and pressure are perpendicular; therefore, baroclinic production of vorticity is expected for both S1 and S2 cases, but the higher magnitude of the density gradient in S2 triggers an instability. The second mechanism is the Darrieus–Landau Instability (DLI), which was identified as the cause of large-scale flame wrinkling

Table 3
Flame Surface Σ computed at an isosurface of $T = 0.7\,T_{\text{ad}}$ for simulations S1, S2 and S3.

	S1	S2	S3
Σ [cm^2]	18.83	35.64	10.92

in both [7,8]. Both instability mechanisms share the same growth factor σ, for which values are reported in Table 2. Note that, in the present case, the characteristic tulip-shaped structure of DLI is not observed, as it would require a free propagation of the products to achieve.

4.3. Effect of equivalence ratio at low temperature

The effect of decreasing the equivalence ratio from $\phi = 5$ to 3 at the low-injection temperature is discussed here (simulation S3 of Table 2). From first principles, the higher density ratio between reactants and products at this lower equivalence ratio, as shown in Table 2, would typically lead to stronger Darrieus–Landau (DL) instability. However, the increased flame speed and reduced flame thickness stabilize the flame, bringing its regime back to a configuration similar to the baseline case S1, as highlighted by the contour of variance of HRR shown in Fig. 6. This is further observed by looking at temperature evolution data for the three cases S1 to S3 in Fig. 7, where strong fluctuations of the order of 200 K are observed for case S2. Although a higher mean temperature is achieved for case S3 as compared to cases S1 and S2, intense fluctuations are not observed in this case despite the low temperature injection.

Further insight can be provided by analyzing the flame surface for the three cases. Values of time averaged flame surface are reported in Table 3.

The corresponding freely propagating premixed flames for cases S1, S2 and S3, obtained from 1D computations at the same injection conditions, would produce an amount of NO as reported in Table 2. In case S3, the sensible reduction in flame surface is counterbalanced by the exponential nature of thermal NO_x formation, which increases NO mass fraction by one order of magnitude as compared to S1. Even with such a strong reduction in flame surface for case S3 (Σ halves as compared to case S1 and is more than three times smaller than that for case S2), by assuming in first analysis that the flamelet NO mass fraction corresponds to the amount of NO mass fraction produced per unit surface, a decrease in equivalence ratio is therefore expected to be insufficient to mitigate NO emissions. In the context of an RQL design, however, a lower rich equivalence ratio may require a shorter mixing length, potentially reducing pressure losses while still maintaining reasonable levels of NO produced, attained by the use of low-temperature injection without the risk of high-magnitude temperature fluctuations.

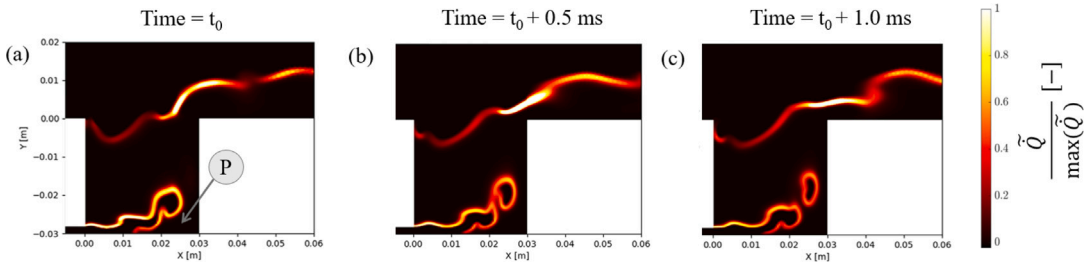

Fig. 5. Midplane contours of heat release rate from LES-ESF model for case S2 of Table 2 for different instant of times starting from time t_0. The label P indicates a probe used in a subsequent analysis.

Fig. 6. Midplane contours of normalized variance of HRR in the cavity cases for simulations S1 (left), S2 (center) and S3 (right) of Table 2.

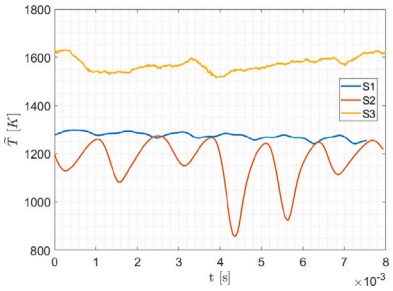

Fig. 7. Instantaneous temperature signal from a probe placed in ($x = 25$ mm, $y = -28$ mm), marked by the label P in Fig. 5.

5. Conclusions

Large eddy simulations (LES) using the Eulerian stochastic fields (ESF) approach were conducted to investigate the combustion physics within a trapped vortex cavity (TVC) configuration for a rich premixed H_2/air flame. In particular, the injection temperature of the H_2/air mixture into the cavity was reduced to 150 K to assess its effect on flame dynamics and NO emissions.

The accuracy of the LES is first assessed by comparing results obtained with the ESF approach against available experimental data for a methane/hydrogen blend in the same configuration, including OH* chemiluminescence measurements and LES results using an artificial thickened flame (ATF) approach. These comparisons show that the ESF model accurately captures the rich combustion physics within the cavity. A parametric study is then performed to explore the low-temperature rich H_2/air combustion. Results show that lowering the injection temperature from 300 K to 150 K at a very rich equivalence ratio of $\phi = 5$ leads to strong flame oscillations, characterized by enhanced flame wrinkling. These instabilities are primarily driven by the interplay of Darrieus–Landau instabilities and baroclinic vorticity generation, which become more prominent due to the increased density of the colder reactants injected in the cavity.

When the equivalence ratio is decreased from $\phi = 5$ to 3 at the same low temperature injection of 150 K, flame oscillations are suppressed, bringing the flame dynamics back to stability. However, this stabilization comes at the cost of an increased adiabatic flame temperature, although temperatures remain below 1700 K. This increase of NO is however counterbalanced by a strong reduction in flame surface, which halves that of the baseline case at 300 K, indicating that despite the increase due to temperature, NO_x formation remains relatively controlled.

These findings highlight that low-temperature rich injection within a TVC can be advantageous to mitigate between flame stability and emissions, which is particularly relevant for rich-quench-lean (RQL) type combustors. Nevertheless, the strong diffusivity of hydrogen in such an RQL system with TVC would lead to the formation of a spurious diffusion flame in the shear layer between cavity and air flow, and how to avoid this formation is the object of future studies.

CRediT authorship contribution statement

Lorenzo Mazzei: Writing – review & editing, Writing – original draft, Supervision. **Ivan Langella:** Writing – review & editing, Writing – original draft, Supervision, Conceptualization. **Vittorio De Lauso:** Conducted simulations and data analysis, Writing – original draft.

Novelty and significance statement

The novelty lies in exploring hydrogen combustion within a trapped vortex combustor, particularly in a low-temperature, premixed hydrogen-rich regime, which is an unusual operating setting. The study extends the corroborated knowledge on laminar rich premixed hydrogen/air flames and it provides an application of said flames in a test-rig type combustion chamber. The trapped vortex combustor provides an effective approach to reduce NOx emissions, while maintaining low pressure losses and a compact size, making it a promising solution for next-generation aerospace propulsion systems, and a significant addition to the literature on this setup.

Declaration of competing interest

The authors declare that they have no known competing financial interests or personal relationships that could have appeared to influence the work reported in this paper.

Acknowledgments

This project has received funding from the European Union's Horizon Europe Research and Innovation Programme under grant agreement No. 101138960, project TRIATHLON. This work used the Dutch national e-infrastructure with the support of the SURF Cooperative using grant no. EINF-11818. EuroHPC JU is acknowledged for awarding the project ID EHPC-REG-2024R01-064 access to MeluXina CPU in Luxembourg. The work is carried out in the framework of the Regular Access project FULCRUMS. The CONVERGE licenses used in this work were obtained through the CONVERGE Academic Program.

Appendix A. Supplementary data

Supplementary material related to this article can be found online at https://doi.org/10.1016/j.proci.2025.105865.

References

[1] D. Zhao, E. Gutmark, P. de Goey, A review of cavity-based trapped vortex, ultra-compact, high-g, inter-turbine combustors, Prog. Energy Combust. Sci. 66 (2018) 42–82.
[2] A.L. Sánchez, F.A. Williams, Recent advances in understanding of flammability characteristics of hydrogen, Prog. Energy Combust. Sci. 41 (2014) 1–55.
[3] Q. Zeng, X. Chen, Combustor technology of high temperature rise for aero engine, Prog. Aerosp. Sci. 140 (2023) 100927.
[4] N. Verma, R. Ravikrishna, Experimental studies on lean blowout limits for a hydrogen-enriched methane-fueled trapped vortex combustor, in: Turbo Expo: Power for Land, Sea, and Air, vol. 87943, 2024, V03AT04A071.
[5] D.L. Straub, K.H. Casleton, R.E. Lewis, T.G. Sidwell, D.J. Maloney, G.A. Richards, Assessment of rich-burn, quick-mix, lean-burn trapped vortex combustor for stationary gas turbines, J. Eng. Gas Turbines Power 127 (1) (2005) 36–41.
[6] D. Veynante, L. Vervisch, Turbulent combustion modeling, Prog. Energy Combust. Sci. 28 (3) (2002) 193–266.
[7] L. Yang, Z. Chen, Effects of cryogenic temperature on premixed hydrogen/air flame propagation in a closed channel, Proc. Combust. Inst. 39 (3) (2023) 2991–2999.
[8] C. Chen, C. Chi, D. Thévenin, W. Han, L. Yang, Effects of cryogenic temperature on turbulent premixed hydrogen/air flames, Proc. Combust. Inst. 40 (1–4) (2024) 105749.
[9] D.C. Haworth, Progress in probability density function methods for turbulent reacting flows, Prog. Energy Combust. Sci. 36 (2) (2010) 168–259.
[10] J.-P. Legier, T. Poinsot, D. Veynante, Dynamically thickened flame LES model for premixed and non-premixed turbulent combustion, in: Proceedings of the Summer Program, vol. 12, 2000, pp. 157–168.
[11] T. Butler, P.J. O'Rourke, A numerical method for two dimensional unsteady reacting flows, in: Symposium (International) on Combustion, vol. 16, Elsevier, 1977, pp. 1503–1515.
[12] S.L. Michaux, K.P. Chatelain, W.L. Roberts, D.A. Lacoste, Laminar burning velocities of hydrogen-air and methane-air flames from ambient to cryogenic temperatures at different equivalence ratios, Int. J. Hydrog. Energy 100 (2025) 608–616.
[13] F. Nicoud, F. Ducros, Subgrid-scale stress modelling based on the square of the velocity gradient tensor, Flow Turbul. Combust. 62 (3) (1999) 183–200.
[14] W. Sutherland, LII. The viscosity of gases and molecular force, Lond. Edinb. Dublin Philos. Mag. J. Sci. 36 (223) (1893) 507–531.
[15] C. Dopazo, E.E. O'Brien, An approach to the autoignition of a turbulent mixture, Acta Astronaut. 1 (9–10) (1974) 1239–1266.
[16] L. Valino, R. Mustata, K.B. Letaief, Consistent behavior of Eulerian Monte Carlo fields at low Reynolds numbers, Flow Turbul. Combust. 96 (2016) 503–512.
[17] N. Kornev, E. Hassel, Method of random spots for generation of synthetic inhomogeneous turbulent fields with prescribed autocorrelation functions, Commun. Numer. Methods Eng. 23 (1) (2007) 35–43.
[18] A. Kazakov, M. Frenklach, Reduced reaction sets based on GRI-Mech 1.2: 19-species reaction set, 2019.
[19] A.A. Konnov, Yet another kinetic mechanism for hydrogen combustion, Combust. Flame 203 (2019) 14–22.
[20] K. Richards, P. Senecal, E. Pomraning, Converge 3.0. Convergent science, 2021, Madison, WI.
[21] H.G. Weller, G. Tabor, H. Jasak, C. Fureby, A tensorial approach to computational continuum mechanics using object-oriented techniques, Comput. Phys. 12 (6) (1998) 620–631.
[22] D. Rockwell, E. Naudascher, Self-sustaining oscillations of flow past cavities, J. Fluids Eng. (1978).